14th IEA Heat Pump Conference
15-18 May 2023, Chicago, Illinois

Ionic liquid absorption system for dehumidification and IAQ enhancement in built environment

Rohit Bhagwat[a], Michael Schmid[b], Abbas Ahsan[c], Navin Kumar[c], Paul Glanville[c], and Saeed Moghaddam[a*]

[a]University of Florida, 939 Sweetwater Dr, MAE-A Bldg, RM 310, Gainesville, FL, 32611, USA
[b]Micro Nano Technologies, 747 SW 2nd Ave, Gainesville, FL, 32601, USA
[c]GTI Energy, 1700 S Mt Prospect Rd, Des Plaines, IL, 60018, USA

Abstract

Cooling systems are a necessity of modern civilization that have greatly enhanced our standard of living and enabled the development of large population centers in harsh climates. However, a key shortcoming of the existing prominent cooling system i.e., vapor compression system is the need for overcooling of air to condense its moisture content. This limitation often leads to implementation of reheat to bring the air to a desired supply temperature to maintain comfort and indoor air quality (IAQ). Liquid desiccant absorption systems have been considered to handle the latent load such that need for reheat is eliminated. However, a low energy efficiency, high cost, and operational and maintenance complexities have prevented such systems from becoming a mainstream product. Here, we report progress on development of ionic liquid desiccant dehumidification systems with a membrane-based absorber that promise to overcome shortcomings of the existing desiccant dehumidification systems. We compare performance of the system operating with adiabatic and internally cooled membrane-based absorbers. The studies are conducted at Integrated Seasonal Moisture Removal Efficiency (ISMRE) inlet air conditions. Effect of dew point temperature on system capacity and coefficient of performance (COP) is studied. A maximum COP of 0.82 is reached, showing promise in terms of energy efficiency. The studies also suggest that further enhancement in dehumidification level is required to meet the needs of HVAC systems.

Selection and/or peer-review under the responsibility of the organizers of the 14th IEA Heat Pump Conference 2023.

Keywords: Absorption; Dehumidification; Liquid desiccant; Ionic liquid

1. Introduction

Cooling systems are responsible for nearly 10% of the global electricity consumption [1]. This energy use is steadily rising due to the increase in the number of installed cooling systems and climate temperature. Currently, only 8% of the 2.8 billion people living in the hottest parts of the world possess an air conditioner [1]. As the living standard in these areas rises, the number of air conditioners is expected to increase [2]. It is projected that the global energy consumption associated with cooling could reach 6,200 TWh by year 2050 [1]. The use of dedicated outdoor air systems (DOAS) for applications with large ventilation loads have shown reduction in the overall building energy use and improvements in the indoor air quality (IAQ). A DOAS is designed to handle the outdoor ventilation air latent load. However, to remove moisture from air, vapor compression systems must overcool air to saturation conditions. The use of a more thermodynamically efficient process to remove moisture from air has the potential to improve energy efficiency in HVAC systems.

In this study, an experimental analysis of a membrane-based ionic liquid (IL) desiccant dehumidification system is presented. This work builds upon our invention of specific aspects of this absorption cycle [4,5] and demonstration of its performance using ILs [5–7] as well as characterization of a membrane-based absorber for dehumidification [8,9]. In the following sections, the system configuration, and its components, including

* Corresponding author. *E-mail address:* saeedmog@ufl.edu

the absorber, desorber, and the implemented IL are introduced. The experimental system is presented, and measurement uncertainties are discussed. The system dehumidification performance is measured at the Integrated Seasonal Moisture Removal Efficiency (ISMRE) inlet air conditions used to establish dedicated outdoor air systems (DOAS) performance characteristics.

2. Experimental System

2.1. Process and instrumentation diagram

A single-effect liquid desiccant absorption dehumidification system was fabricated and integrated into a test suite (Figure 1). This system operates in a cycle in which water vapor is absorbed from the airflow in the absorber and is subsequently liberated in the desorber (via heating). Within the absorber, the concentrated desiccant solution flows down the absorber plate while interfacing with the airflow through the membrane. The water vapor is absorbed by the solution. The dilute (i.e., water-rich) solution then exits the absorber and is pumped to the desorber where it is regenerated. A heat exchanger (i.e., solution heat exchanger, SHX) recovers heat of the desorber outbound solution to elevate temperature of the desorber inbound solution. This internal energy recovery stage plays a key role in energy efficiency of the system as well as absorber performance, as it lowers the absorber inlet solution temperature. The water vapor liberated from the solution is condensed, metered, and drained.

This experimental test setup consists of two primary flow loops including the solution and airflow loops as well as three secondary flow loops; the heating oil loop, the condenser/absorber cooling water loop, and the air-cooling loop (cf. Figures 1 and 2). The IL solution exiting the absorber is pumped to the desorber by a small variable speed gear pump. The absorber is located within the closed air loop (cf. Figure 2). To control the humidity level within the air loop, a steam generator in conjunction with a custom-made steam distribution manifold are utilized. To control the air temperature, a secondary water loop is connected to a heating/cooling coil installed within the air duct. A variable speed axial fan is used to circulate air through the air loop. The heating oil loop, which powers the desorber, utilizes a heating oil bath and synthetic oil SIL 180. An additional water chiller is used to cool the absorber (in inter-cooled operation) and the condenser. Temperature, relative humidity, and flow sensors (Figure 1) are installed throughout the system to enable components and system level characterizations.

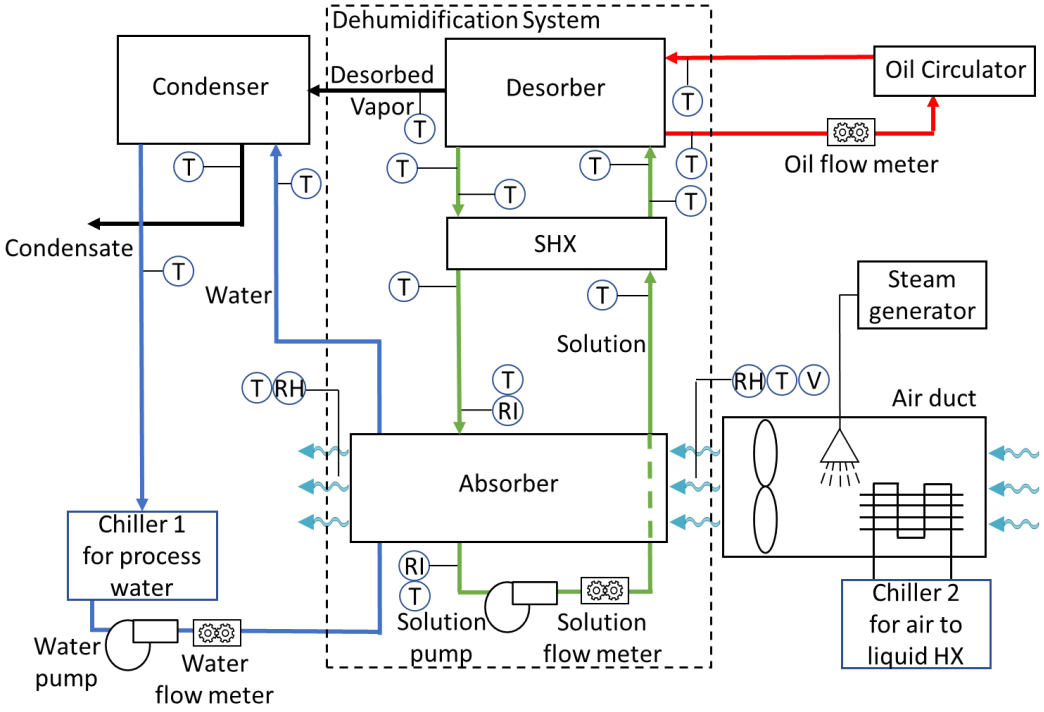

Figure. 1. Process and instrumentation diagram of the experimental test system.

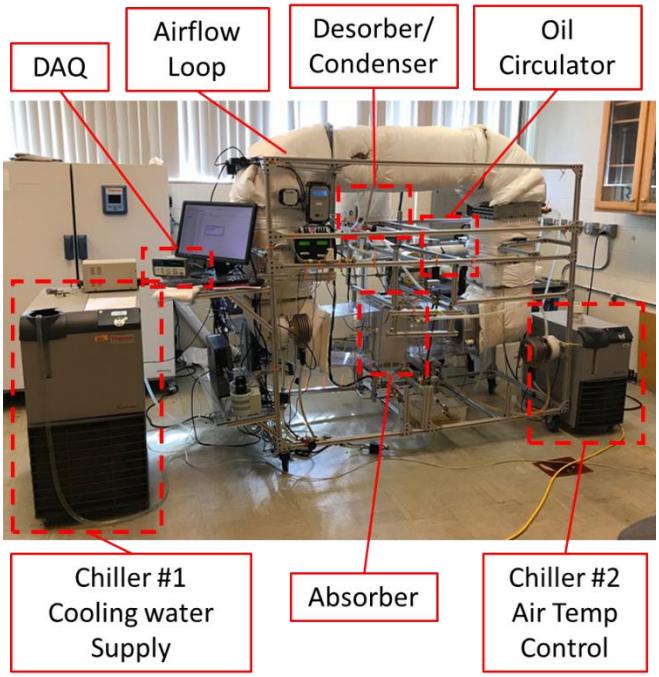

Figure. 2. Photograph of the experimental system with the key components identified.

2.2. Absorber

A schematic of an absorber panel showing the desiccant solution, cooling water, and airflow is shown in Figure 3. The absorber is fabricated from Acrylonitrile Butadiene Styrene (ABS) sheets. Each absorber plate has an internal cooling water core containing water channels and distribution manifolds. The desiccant solution flows on the two outer surfaces of each plate. The plate surfaces are machined to include features designed to slow and spread the solution flow to "wet" the entire surface (front and back) of each sheet [10,11]. A membrane is then bonded over the surface features to constrain the solution. Lastly, manifolds are bonded on the top and bottom of each side of the ABS sheet-membrane assembly (i.e., a panel) to direct the IL flow through the gap formed in between the ABS surface and membrane, and the water to the internal water cavity. Air flows across the panels (cf. Figure 3) through 3 mm gaps formed in between them within the absorber assembly. Geometrical characteristics of the absorber is listed in Table 1.

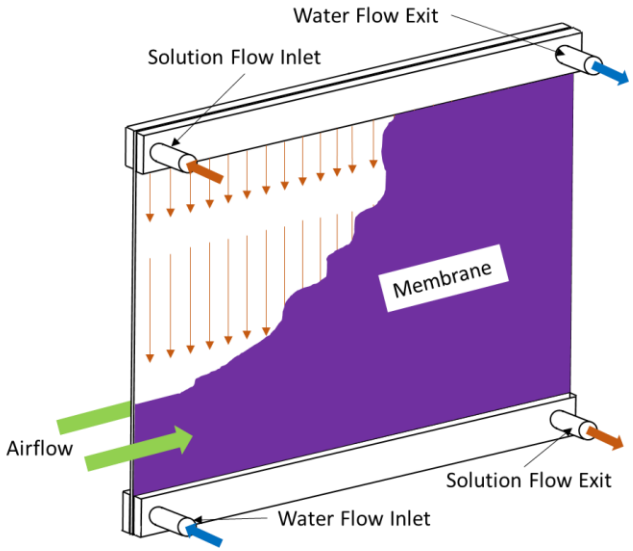

Figure 3. A schematic of a single absorber plate showing airflow across the membrane while exchanging moisture with the desiccant solution constrained behind the membrane.

Table 1. Absorber geometrical characteristics

Parameter	Value
Number of panels	14
Active Surface area (m^2)	3.30
Active plate Volume (m^3)	0.0091
Active surface area/volume ratio (m^{-1})	363.6

2.3. Desorber and Condenser

Figure 4 depicts the desorber, showing the dilute solution supplied by a distribution manifold over the desorber surface. To ensure uniform supply of solution over the surface (Figure 4A) and enhancement of the desorption rate, surface structures described in our earlier studies are utilized here [12]. The desorber surface is heated using silicone oil in a counter flow heat exchange configuration (Figure 4A). To capture and condense the vapor, a condensing surface is built adjacent to the desorber surface, separated by a porous polytetrafluoroethylene (PTFE) membrane (Figure 4B). A critical function of this membrane is to eliminate IL carryover from the desorber while permitting water vapor migration to the condensing surface. The condensing surface is cooled using a water loop.

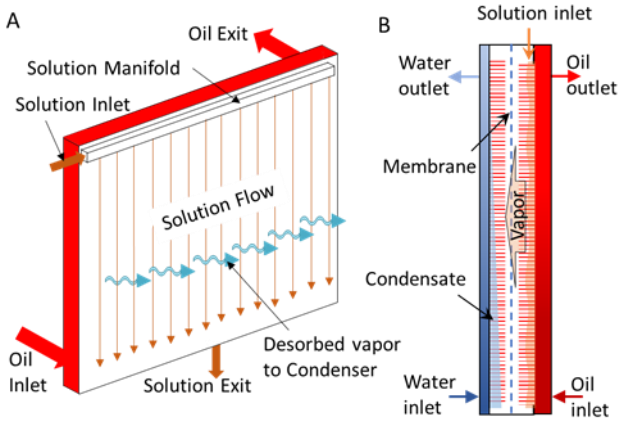

Figure 4. A schematic of the desorber and condenser assembly showing solution falling film flow configuration (A) and the desorption of water vapor, its flow through a PTFE membrane, and subsequent condensation in the condenser (B).

2.4. Measurement System

The solution flow rate is measured using a positive displacement flow meter. Due to the elevated temperature of the oil flow loop, a high-temperature positive displacement flow meter is used to measure the oil flow rate. The water flow rate is measured using a turbine flow meter. All flow meters were calibrated in house using a bucket-stopwatch method. The airflow rate is measured using a pitot tube sensing element mounted within the air loop duct. Multiple sensing ports along the length of the sensing element are used, and internally averaged to ensure accurate airflow rate measurement. All liquid temperatures were measured using T-type thermocouples. The process air temperature and relative humidity are measured using thin-film capacitive sensors. The absorber solution inlet and outlet concentrations are measured using two inline refractive index (RI) sensors. RI instead of Coriolis effect is used because the variation in density for ILs is insignificant over a wide concentration range, making accurate measurement of the concentration infeasible. Curve fits have been developed to establish RI values as a function of IL concentration and temperature. The primary system temperature, flow rate, RI, and air velocity are recorded using a data acquisition system. A second data acquisition system is used to record the air temperature and relative humidity. Time stamps are used to combine the data collected by each data acquisition system to enable a system level data analysis.

2.5. Data reduction and uncertainty analysis

The system performance presented in the results and discussion section is calculated based on the measured data described above. The system latent capacity is calculated using Eq. (1).

$$Q_{latent} = \dot{V}_{air}\, \rho_{air}\, h_{fg}\, (\omega_{air\_in} - \omega_{air\_out}) \quad (1)$$

where $\dot{V}_{air}$ is the absorber airflow rate; ω_{air_in} and ω_{air_out} are the absorber air inlet and exit absolute humidity, respectively; ρ_{air} is the air density as calculated from standard tables using the measured air inlet conditions; and h_{fg} is the water latent heat of evaporation. The desorber heat input is calculated using Eq. (2).

$$Q_{oil} = \dot{V}_{oil}\, \rho_{oil}\, c_{p\_oil} (T_{des\_oil\_in} - T_{des\_oil\_out}) \quad (2)$$

where $\dot{V}_{oil}$ is the desorber oil flow rate; $T_{des\_oil\_in}$ and $T_{des\_oil\_out}$ are the desorber oil inlet and outlet temperatures, respectively; ρ_{oil} is the oil density; and c_{p_oil} is the oil thermal capacity calculated using curve fits derived from data provided by Clearco for their SIL 180 silicone oil. The system latent heat capacity along with the desorber heat input are used in Eq. (3) to calculate the system COP.

$$COP = \frac{Q_{latent}}{Q_{oil}} \quad (3)$$

The absorber moisture removal rate (MRR) is calculated using Eq. (4).

$$MRR = \dot{V}_{air}\, \rho_{air}\, (\omega_{air\_in} - \omega_{air\_out}) \quad (4)$$

The uncertainty was calculated using an engineering equation solver (EES) uncertainty propagation subroutine. The subroutine is based on NIST guidelines[13] and assuming that the individual measurements are uncorrelated and random, the uncertainty in the calculated quantity can be estimated using Eq. (5).

$$U_Y = \sqrt{\sum_i \left[\frac{\partial Y}{\partial X}\right]^2 U_{X_i}^2} \quad (5)$$

Table 2 below lists all the relevant measurement errors and uncertainties in this experimental study.

Table 2. Measurement error and uncertainty propagation.

Variable	Uncertainty
Fluid temperatures -All T-type TC	±0.8°C
Solution volumetric flow rate	±0.25% reading
Solution RI	±0.5% scale range (0.0003nD)
Water volumetric flow rate	±1% full scale (0.5 LPM)
Air volumetric flow rate	±2% reading
Oil volumetric flow rate	±0.5% reading
Air temperature	±0.3% reading
Air relative humidity	±1.8% RH
Oil heat	±3.7%
Water heat	±2.0%
Concentration (X%)	±0.15%
COP	±4.2%

2.6. Test Conditions

The test conditions listed in Table 3 represent the ISMRE [14] inlet air conditions used to establish DOAS performance characteristics. The inlet air, IL solution, and oil flow rates as well as the oil inlet temperature have been held constant at 155 cfm, 300 mlpm, 2.85 lpm, and 148 °C, respectively.

Table 3. Inlet air test conditions.

Test Condition	Inlet Air Conditions			Notes
	Dry Bulb Temp [°C]	Dew Point Temp [°C]	Rel. Hum. [%]	
1	35.0	22.1	47.29	ISMRE A
2	26.7	21.2	72.03	ISMRE B
3	21.1	17.8	81.36	ISMRE C
4	17.2	13.6	79.41	ISMRE D

3. Results

Figure 5 shows results of a typical run conducted at the ISMRE A test condition operating with an intercooled absorber at an air inlet temperature of ~35 °C and ~52% relative humidity. It is noted that due to the low thermal mass of the system, the system quickly reaches steady state conditions. In these steady state conditions, the difference in the inlet and exit air absolute humidity remains constant (Figure 5A), resulting in an essentially constant moisture removal rate (Figure 5B).

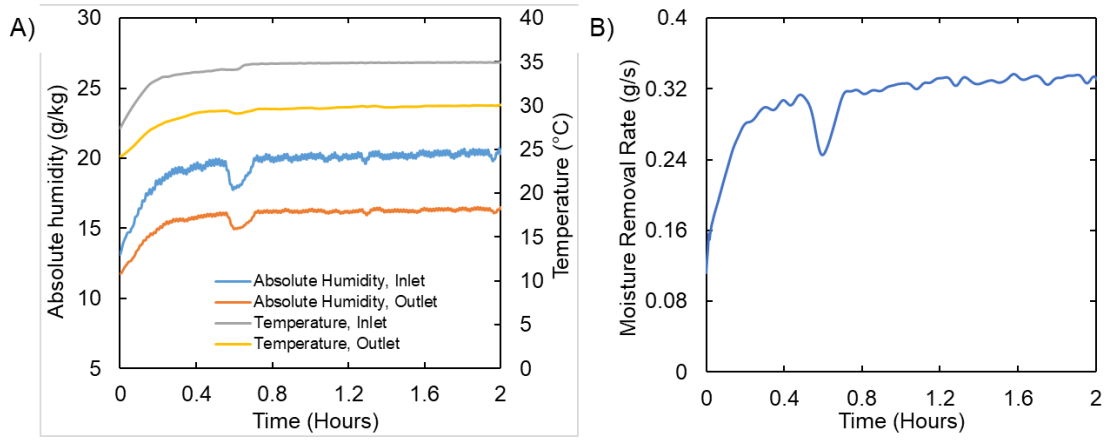

Figure 5. System inlet and exit air conditions (a) and water removal (b) with an intercooled absorber at ISRME A conditions. The inlet air, IL solution, and oil flow rates as well as the oil and water inlet temperatures have been held constant at 155 cfm, 300 mlpm, 2.85 lpm, 148 °C, and 10 °C, respectively.

3.1. Dehumidification performance

The dehumidification performance of the system was experimentally evaluated at each of the four ISRME test conditions, with the absorber operating in both adiabatic and intercooled configurations. In these flow configurations, the water flow rate was varied between 0 lpm (no flow) and 0.82 lpm for the adiabatic and intercooled configurations, respectively. The absorber inlet water temperature for the intercooled condition was held constant at 10 °C. The dehumidification performance of the system is plotted on the psychometric chart shown in Figure 6. In the adiabatic configuration, the heat associated with condensation of the water vapor into the solution is returned to the air stream. As a result, the air is dehumidified and heated in a nearly isenthalpic process. In the intercooled configuration, the absorber heat energy is removed by the cooling water enabling latent and sensible cooling of the process air.

Typically, in DOAS applications, outdoor ventilation air is dehumidified and conditioned to a room or neutral state (Figure 6). As can be seen, dehumidification of the process air to neutral conditions was not achieved during these tests. For ISMRE conditions C and D, it is believed that slight changes in the water and airflow rates will enable the existing system to deliver neutral air. For ISMRE conditions A and B, in addition to changes to air and water flow rates, a larger absorber is required. This experiment demonstrated that this absorber configuration, with proper air/water flow control can provide a wide range of air conditioning (above isenthalpic to constant relative humidity cooling). This range of air conditioning is enabled by the dehumidification capacity of the solution and the heat transfer between the absorber fluids. This is exemplified by performing above isenthalpic dehumidification because of the additional sensible heat transfer from the solution to the air emanating from high temperature of the solution entering the absorber.

The absorber implemented for this test, was approximately 35 cm tall, 35 cm long, and 8 cm wide with an active surface area of 3.3 m2 (Table 1). The dehumidification capacity, in latent cooling (W) and the moisture removal rate (kg/hr) of the absorber in the two configurations is shown in Figure 7. As shown in Figure 7, the dehumidification performance of the intercooled configuration is significantly better than that of the adiabatic configuration. The water absorption process is driven by the difference in vapor pressure between the process air and the desiccant solution. As the desiccant solution is heated its vapor pressure increases, reducing the absorption rate. As the cooling water in the intercooled configuration cools the solution, it is intuitive that under the same physical conditions (size, surface area, flow rates, etc.) the intercooled configuration will have a greater dehumidification capacity than the adiabatic configuration. As the architecture of both the absorber and desorber are modular, the addition of plates serves to increase system capacity.

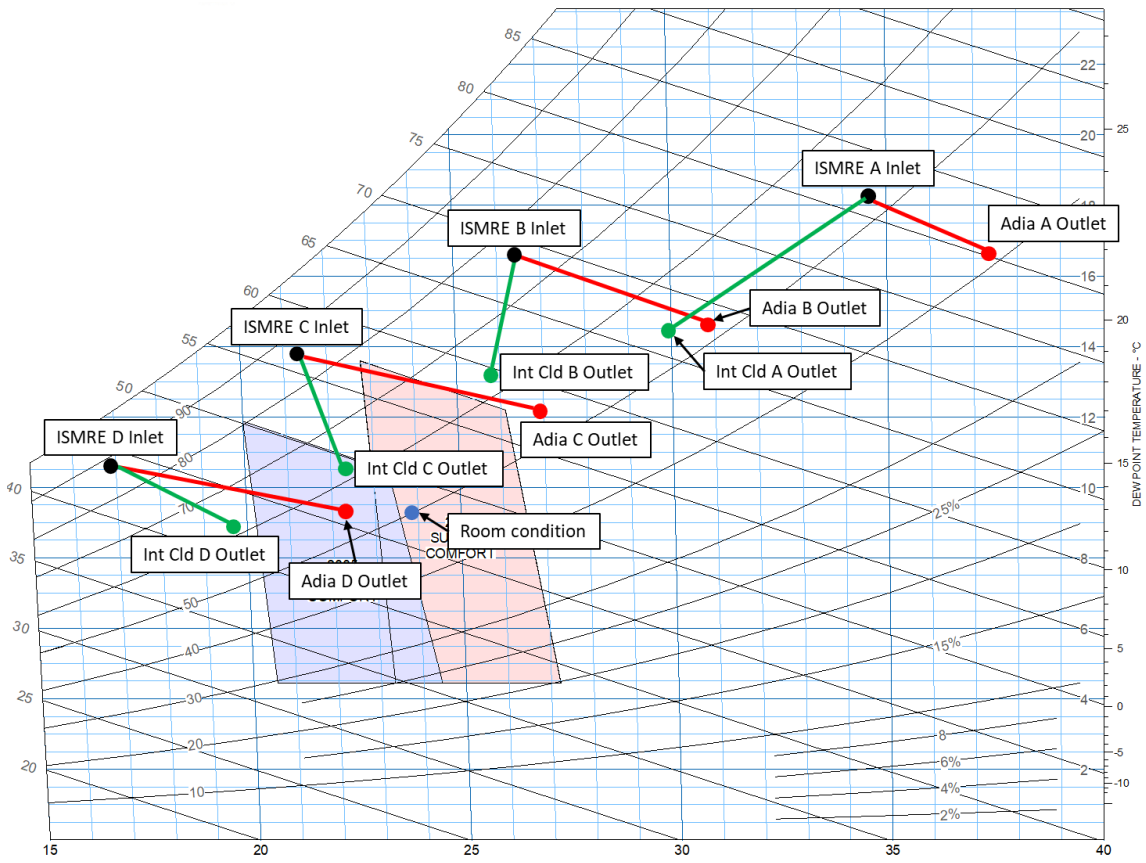

Figure 6. System inlet and exit air conditions for the system operating in the adiabatic and intercooled configurations at the four ISMRE conditions. The inlet air, IL solution, and oil flow rates as well as the oil and water inlets temperature have been held constant at 155 cfm, 300 mlpm, 2.85 lpm, 148 °C, and 10 °C, respectively.

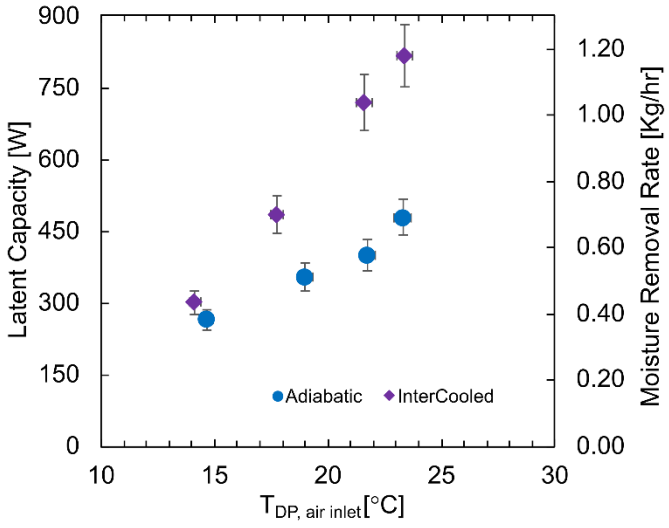

Figure 7. System latent capacity and moisture removal rate as a function of inlet air dewpoint temperatures which approximate the ISMRE conditions for the adiabatic and intercooled absorber configurations. The inlet air, IL solution, and oil flow rates as well as the oil and water inlet temperatures have been held constant at 155 cfm, 300 mlpm, 2.85 lpm, 148 °C and 10°C, respectively.

3.2. Coefficient of performance (COP)

As the primary function of the system is dehumidification, its COP (calculated using Eq. 3) represents the system's dehumidification (latent cooling) efficiency. This COP is plotted in Figure 8 as a function of the inlet

air dew point temperatures representative of the four ISMRE conditions. As shown in Figure 8, the COP of the system with the intercooled absorber (chilled water inlet temperature of 10 °C) is greater than that of the adiabatic configuration at higher dewpoint temperatures. The highest COP is associated with the maximum latent load, as dew point temperature is an indicator of the air moisture content. Although the system performance is presented in Figure 8 as a function of the inlet air dew point temperature, the inlet water and air drybulb temperatures also impact system performance. For the intercooled absorber, the inlet chilled water temperature has been maintained as 10 °C, which cools the solution within the absorber, ultimately resulting in the absorber inlet temperature being held essentially constant across the four test conditions. In contrast, the solution inlet temperature of the adiabatic absorber increases with increasing air inlet dewpoint/drybulb temperatures, such that for ISMRE A (22.1 °C $T_{DP, air\ inlet}$) it is 15 °C higher than its intercooled counterpart. While the cooling water dominates the heat transfer characteristics of the absorber, cooling both the solution and the air, the air inlet dry bulb temperature increased the solution temperature within the adiabatic absorber. The resulting increase in solution temperature decreased the latent capacity of the adiabatic absorber relative to the intercooled absorber at the higher inlet air dewpoint/drybulb conditions.

As shown in Figure 8, the system COP declines, regardless of absorber configuration, as the inlet air dewpoint temperature decreases. The system performance at these low dewpoint conditions was negatively impacted by maintaining a constant solution flow rate. The COP is expected to improve by lowering the solution flow rate such that change in the solution concentration between the absorber inlet and outlet is maximized. In other words, the solution flow rate should match the air dehumidification requirement.

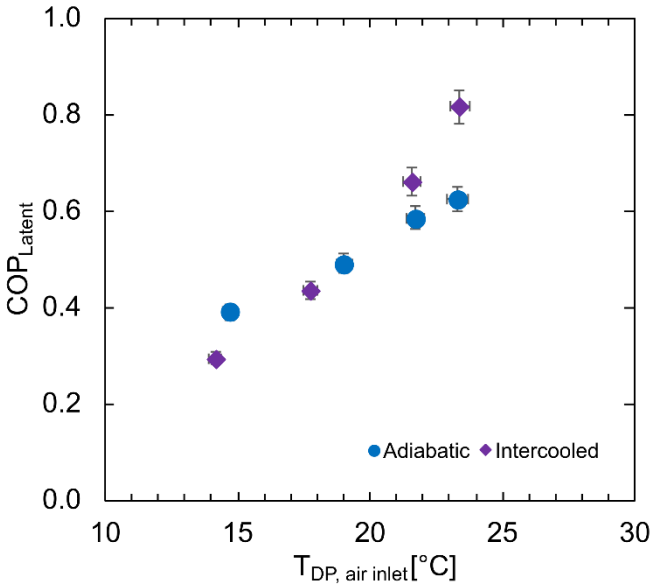

Figure 8. System COP as a function of air inlet dew point temperatures that approximate the ISMRE condition for the adiabatic and intercooled absorber configuration. The inlet air, IL solution, and oil flow rates as well as the oil and water inlet temperatures have been held constant at 155 cfm, 300 mlpm, 2.85 lpm, 148 °C, and 10°C, respectively.

4. Conclusions

A lab scale IL dehumidification system was experimentally tested in two configurations, adiabatic and intercooled, at the inlet air conditions representative of the four ISMRE test conditions, while the system internal operating conditions were maintained constant. The use of IL demonstrated the robustness of the system in providing dehumidification across a wide operational range, without control equipment for mitigating crystallization. An all polymer plate-and-frame membrane-based absorber effectively demonstrated dehumidification of the airflow in a small volume format. The measured system latent performance and system COP ranged from ~265 W to ~820 W, and 0.30 to 0.82 respectively across the test conditions. These tests demonstrated that this absorber configuration, with proper air/water flow control can provide a wide range (beyond isenthalpic to constant relative humidity cooling) of air conditioning, which when properly sized can deliver ventilation air at neutral air conditions.

Nomenclature

ABS	acrylonitrile butadiene styrene
Adia	adiabatic
CFM	cubic feet per minute
COP	coefficient of performance
D	depth
H	height
HX	heat exchanger
IL	ionic liquid
ISMRE	integrated seasonal moisture removal efficiency
Int Cld	intercooled
L	length
LPM	liters per minute
mLPM	milliliters per minute
PTFE	Polytetrafluoroethylene
RI	refractive index
RH	relative humidity
SHX	solution heat exchanger
$\dot{m}$	mass flow rate (kg/sec)
T	temperature (°C)
$T_{DP,in}$	Inlet air dew point temperature (°C)
TWh	terawatt hour
V	volumetric flow rate

Acknowledgements

This work was sponsored by the U. S. Department of Energy, Office of Energy Efficiency and Renewable Energy (EERE), under Award Number DE-EE0009162 with the University of Florida. The authors would also like to acknowledge Mr. Antonio Bouza, Ms. Coriana Fitz, and Dr. Isaac Mahderekal from the U.S. DOE Building Technologies Office (BTO) for their support of this research.

References

[1] OECD/IEA. The Future of Cooling Opportunities for energy-efficient air conditioning Together Secure Sustainable 2018:92.

[2] Davis L, Gertler P, Jarvis S, Wolfram C. Air conditioning and global inequality. Global Environmental Change 2021;69:102299. https://doi.org/10.1016/j.gloenvcha.2021.102299.

[3] Woods J, James N, Kozubal E, Bonnema E, Brief K, Voeller L, et al. Humidity's impact on greenhouse gas emissions from air conditioning. Joule 2022:1–16. https://doi.org/10.1016/j.joule.2022.02.013.

[4] Moghaddam S, Chugh D, Nasrisfahani R, Bigham S, Fazeli SA, Yu D, et al. Open absorption cycle for combined dehumidification, water heating, and evaporative cooling, 2018.

[5] Gluesenkamp KR, Chugh D, Abdelaziz O, Moghaddam S. Efficiency analysis of semi-open sorption heat pump systems. Renew Energy 2016:1–10. https://doi.org/10.1016/j.renene.2016.07.075.

[6] Chugh D, Gluesenkamp K, Abdelaziz O, Moghaddam S. Ionic liquid-based hybrid absorption cycle for water heating, dehumidification, and cooling. Appl Energy 2017;202. https://doi.org/10.1016/j.apenergy.2017.05.161.

[7] Chugh D, Gluesenkamp KR, Abu-Heiba A, Alipanah M, Fazeli A, Rode R, et al. Experimental evaluation of a semi-open membrane-based absorption heat pump system utilizing ionic liquids. Appl Energy 2019;239:919–27. https://doi.org/10.1016/j.apenergy.2019.01.251.

[8] Bhagwat R, Schmid M, Moghaddam S. Experimental and numerical analysis of a three-fluid membrane-based ionic liquid desiccant absorber. Int J Heat Mass Transf 2022;183:122122. https://doi.org/10.1016/j.ijheatmasstransfer.2021.122122.

[9] Bhagwat R, Sanadhya S, Gulotty E, Tucker Z, Ashfeld B, Moghaddam S. High-precision vapor pressure measurement apparatus with facile and inexpensive construction. Meas Sci Technol

2022;33:067002. https://doi.org/10.1088/1361-6501/ac5135.
[10] Mortazavi M, Isfahani Nasr R, Bigham S, Moghaddam S. Absorption characteristics of falling film LiBr (lithium bromide) solution over a finned structure. Energy 2015;87:270–8.
[11] Nasr Isfahani R, Bigham S, Mortazavi M, Wei X, Moghaddam S. Impact of micromixing on performance of a membrane-based absorber. Energy 2015. https://doi.org/10.1016/j.energy.2015.08.006.
[12] Mortazavi M, Schmid M, Moghaddam S. Compact and efficient generator for low grade solar and waste heat driven absorption systems. Appl Energy 2017;198:173–9. https://doi.org/10.1016/j.apenergy.2017.04.054.
[13] Taylor BN, Kuyatt CE. Guidelines for Evaluating and Expressing the Uncertainty of NIST Measurement Results. Technology (Singap World Sci) 1994:2.
[14] AHRI Standard 921-2020. Performance Rating of Direct Expansion-Dedicated Outdoor Air System Units 2021;920.